



## Full Text View

[Volume 29, Issue 4 \(April 1999\)](#)

## Journal of Physical Oceanography

Article: pp. 560–583 | [Abstract](#) | [PDF \(1.08M\)](#)

## Lagrangian Exploration of the California Undercurrent, 1992–95

Newell Garfield, Curtis A. Collins, Robert G. Paquette, and Everett Carter\*

*Department of Oceanography, Naval Postgraduate School, Monterey, California*

(Manuscript received November 25, 1996, in final form April 8, 1998)

DOI: 10.1175/1520-0485(1999)029&lt;0560:LEOTCU&gt;2.0.CO;2

## ABSTRACT

During the period 1992–95, nineteen isobaric RAFOS floats, placed in the California Undercurrent at intermediate depths (150–600 m) off Monterey and San Francisco, California, reveal a region of varying width of subsurface, poleward flow adjacent to the continental margin. The float trajectories exhibit three patterns: poleward flow in the undercurrent; reversing, but predominately alongshore, flow adjacent to the continental margin; and, farther offshore, anticyclonic motion accompanied by slow westward drift. Flow continuity of the undercurrent exists between Pt. Reyes and at least Cape Mendocino with an average speed dependent on the float depth. Speeds were variable, but common features were acceleration occurring to the south of Pt. Arena and deceleration to the north of Cape Mendocino. An important mechanism for floats, and water, to enter the ocean interior from the undercurrent is through the formation of submesoscale coherent vortices.

## 1. Introduction

The California Undercurrent is found adjacent to the continental slope in the subtropical northeastern Pacific Ocean. The undercurrent transports equatorial water poleward such that the waters next to the slope are warmer, saltier, and lower in oxygen than those found farther offshore ([Hickey 1979](#)). The undercurrent has been identified off Baja California ([Wooster and Jones 1970](#)), Vancouver Island ([Freeland et al. 1984](#)), and at many locations in between. The flow continuity has not been observed directly ([Mooers 1989](#)), but is inferred from maps of hydrographic property distributions ([Hickey 1979](#); [Chelton 1984](#); [Lynn and Simpson 1987](#); [Tisch et al. 1992](#)) and from direct observations of poleward flow along the continental margin ([Noble et al. 1987](#); [Huyer et al. 1989](#); [Largier et al. 1993](#); [Collins et al. 1996b](#), [Smith et al. 1996](#)). [Rischmiller \(1993\)](#), using data from an acoustically tracked dropsonde, found that the area of poleward flow off Point

## Table of Contents:

- [Introduction](#)
- [Methods](#)
- [Flow patterns](#)
- [Pressure and temperature](#)
- [Eddy characteristics](#)
- [Discussion](#)
- [Conclusions](#)
- [REFERENCES](#)
- [APPENDIX](#)
- [TABLES](#)
- [FIGURES](#)

## Options:

- [Create Reference](#)
- [Email this Article](#)
- [Add to MyArchive](#)
- [Search AMS Glossary](#)

## Search CrossRef for:

- [Articles Citing This Article](#)

## Search Google Scholar for:

- [Newell Garfield](#)
- [Curtis A. Collins](#)
- [Robert G. Paquette](#)
- [Everett Carter](#)

Sur extended beyond the upper slope to a distance of 200 km from the coast and to a depth of 750–1000 m or greater. Smith et al. demonstrated the presence of the undercurrent through ADCP transections occupied between Pt. Conception, California, and Oregon.

There have been few Lagrangian measurements of the undercurrent. Measurements obtained with surface-tracked parachute drogues in the region off Monterey California (Reid 1962), Baja California (Wooster and Jones 1970), and Oregon (Stevenson et al. 1969) contributed important information on the existence of the undercurrent, but all were short duration deployments with limited spatial extent. RAFOS floats, the latest generation of acoustically tracked Lagrangian floats, provide the ability to tag and track subsurface flow for long distances and long times at reasonable cost. In the eastern Pacific the axis of the sound channel is relatively shallow and it was anticipated that this would allow the use of these floats to study the relatively shallow undercurrent.

In 1992, we began a Lagrangian exploration of the undercurrent. The goals of our program were to measure the path and continuity of the flow and to determine the character of dispersion in the undercurrent. The primary onshore–offshore exchanges for surface and near-surface waters are thought to take place through processes associated with upwelling dynamics and the offshore flowing filaments that appear to be anchored to upwelling centers. Other coastal studies (Schwing et al. 1991; Rosenfeld et al. 1994; Parker 1996; Baltz 1997; Steger et al. 1998, manuscript submitted to *Deep-Sea Res.*, hereafter SSC) have shown that there is an energetic eddy field along the continental margin and shelf. Our investigation sought to examine the role of the California Undercurrent in these continental margin mixing patterns.

This report describes the results of our Lagrangian exploration of the undercurrent from floats deployed during the period from 1992 through 1995. Float deployments and data processing are described in section 2. Individual float trajectories, and pressure and temperature data are presented in sections 3 and 4, respectively. Eddies are characterized in section 5. The discussion and summary of findings are in section 6. Preliminary statistics, including Lagrangian decorrelation scales, are summarized in the appendix.

## 2. Methods

The RAFOS system is described in detail by Rossby et al. (1985, 1986). We describe below only those elements of the RAFOS system that were particular to our experiment. To distinguish our floats, we identify them by number with the prefix “NPS” (for Naval Postgraduate School).

### a. NPS RAFOS floats

Quasi-isobaric RAFOS floats (floats without pressure compensating devices) were used throughout this portion of the experiment. An ideal isobaric float would settle to the specified pressure surface and remain at that pressure, regardless of the surrounding water. However, RAFOS float density depends in part on the glass and end cap thermal expansions. Swift and Riser (1994) noted that the RAFOS operational surface will not coincide with surfaces commonly quantified in oceanographic literature. Goodman and Levine (1990) derived a “response ratio” to quantify how well a float follows either isobaric (response ratio of one) or isopycnal (response ratio of zero) surfaces. The response ratio,  $r = (1 - s)/(1 - s + [N/cg^{-1}])$ , compares the ratio ( $s$ ) of the float’s compressibility to that of seawater and the Brunt–Väisälä frequency ( $N$ ) normalized by  $cg^{-1}$  ( $\approx 3.8 \text{ cyc h}^{-1}$ ). At the target depths for this study the NPS floats had a compressibility ratio of  $s \approx 0.4$  and a response ratio of  $r \approx 0.75\text{--}0.8$ . Most of the variation of the response ratio came from changes in the normalized buoyancy frequency  $[N/cg^{-1}]$ .

All but the first two NPS floats were ballasted at the Deep Ocean Simulation Facility, Naval Civil Engineering Laboratory, Port Hueneme, California. The 1.9-m diameter pressure vessel is operated with filtered tap water rather than distilled water. Our initial ballasting efforts yielded significant variability from the target pressures, which was probably due to the unknown tap water density. We now compensate for this by determining the tank water density before and after each ballast run using a carefully ballasted and weighted RAFOS hull as a hydrometer.

In addition to recording the time of arrival of the acoustic signals from the moored sound sources used for float navigation, our floats recorded temperature and pressure. Temperature and pressure were measured over a 1-s averaging time interval after each listening cycle, which, depending on the mission parameters, meant one to three samples per day. Temperature had a resolution of 0.02°C and an accuracy of 0.05°C. Pressure had a resolution of 2.5 decibar (1 dbar =  $10^4$  Pa, and a change of 1 dbar  $\approx$  1 m vertical change) and an accuracy of 1% full scale.

### b. Float navigation

An acoustic sound source array using Webb Research 183-dB instruments ensonified the region between 34°N (Pt.

Conception, California), and 43°N (Cape Blanco, Oregon), and extending offshore to at least 132°W (Fig. 1). Four NPS sound sources (SS1 to SS4) were initially deployed in August 1992 and were serviced in August 1994. The source just offshore from Pt. Arena, SS4, was eliminated in 1994 because of confused signal reception by floats and shadowing by Pt. Arena. In addition to the NPS sources, a sound source (V1) was installed by the NOAA Pacific Marine Environmental Laboratory (PMEL) in August 1993, near the Juan de Fuca Ridge. The NPS sources originally transmitted acoustic signals three times per day, with each source broadcast staggered by a half hour. The schedule was changed in 1994 to twice per day. The PMEL source also transmits twice per day, broadcasting one-half hour before the NPS sequence. The RAFOS floats were programmed to listen to all sources, allowing for float positioning two or three times per day.

Navigational errors arise from several sources. A “fixed” error is due to the geometry of the solution and the instrument precision. The resolution of the instrument acoustic signal arrival time is 0.3 s. This translates to an error of  $\sim \pm 0.5$  km in any range estimate. The position accuracy factor resulting from this range error and the site geometry, referred to as the dilution of precision (dop), is a multiplier for other errors. Figure 2 contours the dop for navigation using the three southern sound sources in the region where most of our floats operated. A small dop indicates that the solution geometry introduces only a small navigation error. The dop gives a lower bound on the navigation accuracy error that can be expected given the geometry of the solution for the different ranges. Other navigation error arises primarily from the unknown sound speed and clock drift.

The sound sources were all moored at the climatological mean depth of the deep sound channel (sometimes called the SOFAR channel) at each location, 510–590 m (Johnson and Norris 1968). Although the channel depth varies seasonally, the variability is small enough (on the order of tens of meters) that each source remains near the sound channel axis. The float depths (see below) were generally above the sound channel axis. Estimates of sound trajectories from a relatively small angular range indicate that timing errors from different ray paths were probably small. The sound sources are monitored through the NPS Pt. Sur Ocean Acoustic Observatory hydrophone array, a former navy underwater listening station. The standard deviations, after removing linear trends, for arrival times recorded over a two-year period for sources 1, 2, and 3 were, respectively, 0.167 s, 0.162 s, and 0.183 s.

Float clocks were calibrated prior to launch, but clock drift once the float reached thermal equilibrium at depth was not measured. Since floats were typically not recovered, the float clock drift was not known and had to be approximated.

In determining the float position, errors from the unknown sound speed and clock drift cannot be easily distinguished, and a single editing approximation to the source clocks was done to account for both (Paquette 1996). After applying this correction, the absolute uncertainty in position is estimated to be less than 10 km, with the short-term relative error for each float being smaller (generally about 1 km).

Data processing used NPS modified versions of the University of Rhode Island programs. Details of the modifications can be found in Paquette (1996). Following range and position determination, quality control and statistical analyses were done. Different procedures were used to smooth the positions, depending upon the sampling schedule. For floats that sampled multiple times every other day, the data were averaged to obtain single fixes every other day. These positions were then filtered once with a three-point moving average. For floats with fixes evenly spaced with respect to time, position data were filtered twice with a three-point moving triangular filter. In order to develop a consistent dataset, all float data were then interpolated to daily fixes using a cubic spline interpolation, and velocity was determined by differencing these daily positions. Finally, the velocity estimate was also smoothed (once) with a moving three-point triangular filter. The interpolated and smoothed data were used in this paper.

### *c. Experimental design*

Our sampling plan was to launch triads of RAFOS floats in the California Undercurrent. The primary launch site was west of San Francisco (Fig. 1). Here, triads of floats were launched in a triangular pattern 8 km on a side. Two floats were launched above the 1000-m isobath, while the third was launched at the offshore apex of the equilateral triangle.

The first two floats (NPS1 and 2) were programmed for 30-day missions in order to check system operations. Subsequent subsurface mission lengths were increased, first to 60 days, then to 100 or more days (Fig. 3a). Battery capacity determined the number of listening cycles per day. Short duration floats were set to listen every 8 or 12 hours. The longer duration floats listened less frequently with mission lengths of 300 or more days listening every other day.

The choice of the float depth was a compromise between the depth of the undercurrent core, about 100 m (Rischmiller 1993), and the depth of the SOFAR channel axis, about 550 m (Johnson and Norris 1968). A depth of 100 m falls within the thermocline, which we felt was too shallow for reliable acoustic listening. On the other hand, a depth of 550 m would be too deep, possibly below the undercurrent. Consequently, two principal pressures were targeted, first 350 dbar, then later, after we realized the effectiveness of the acoustic transmissions, 275 dbar.

Cruises were not dedicated to float deployments, so launches were conducted as opportunity arose during other research cruises. Our only criterion was that the time interval between float triad launches exceed the Lagrangian timescale. Since we had no Lagrangian measurements, we used the Eulerian decorrelation timescale of 18 days calculated from a current meter at 350 m over the upper slope off Pt. Sur (Collins et al. 1996b). In fact, the interval between launches was significantly greater. Regular deployments began in July 1993 and followed in September and November 1993, January, April, May, and August 1994. There was a bias toward late summer to early winter as illustrated in Figs. 3b and 3c, where the white bars indicate the total float days by year and month.

#### d. Float performance

Our floats exhibited depth holding characteristics similar to those seen by other RAFOS float users (Bower 1994). The mean, median, and standard deviation of daily interpolated pressure values are plotted in Fig. 4. The equilibrium level reached by four floats deviated substantially from the target pressure. NPS 2, 22, and 33 were about 300 dbar too deep, while NPS5 was 200 dbar too shallow.

Once on the equilibrium pressure level, three factors can cause the quasi-isobaric floats to change that level: internal waves, water mass changes, and float mass changes. Internal waves and internal tides have oscillation frequencies that are aliased in the data by the float sampling schedule. The smaller expansion coefficient for the float compared to that for water will tend to reduce the oscillation amplitude.

Indications that a float sank during a mission are a large standard deviation and a large difference between the mean and median depths. NPS 9, 19, and 24 were “slow sinkers” (Bower 1994), showing a constant slow depth increase over the mission period. It is assumed that this sinking was caused by slow leaks in the hollow ballast weight (a one gram change in float mass translates to approximately 40-m depth change). Four floats were “fast sinkers,” undergoing catastrophic sinking. NPS20 and NPS23 sank immediately; NPS33 sank quickly on day 293 of a planned 499-day mission. NPS19 initially acted as a slow sinker, then two days before the end of its scheduled 203-day mission it sank abruptly. Six floats experienced sinking and four of them terminated the subsurface mission when the ambient pressure exceeded a preset allowable value. Other problems were a malfunctioning pressure transducer on NPS14 (the temperature record suggests that it was at a depth of just less than 300 dbar) and intermittent pressure sensor failures on NPS21 and NPS24.

For the other 13 floats, the mean offset from the target pressure was 18 dbar shallow with a standard deviation of 30 dbar. These are the floats in Fig. 4 that have nearly coincident mean and median pressures and small standard deviations.

The observed depth changes and pressure–temperature behavior for the floats that did not leak appear to be real and are due to a float encountering waters of different temperature and density along the route (Collins et al. 1996a). When isopycnals are inclined to the isobaric surface, the buoyancy force on the float will change with changes in the water density and temperature (Swift and Riser 1994). The change in pressure and the change in the thermal expansion coefficients for water and glass affect the balance between the float and the ambient pressure. When the density increases, the float will rise, and vice versa. Notwithstanding, the water temperature record often fluctuates in phase with the pressure record; a sinking float will have a temperature increase. That is because the equilibrium displacement of the float will be less than the isopycnal displacement of the water causing the change in buoyancy. The temperature–pressure relationship for isobaric floats can be used to check whether or not the float density is changing due to water mass change or to leakage. Normally the  $T$ – $P$  scatter will be in a pattern moving orthogonal to the trend of the local water column  $T$ – $P$  relationship. If the  $T$ – $P$  scatter for a float trends with the vertical  $T$ – $P$  trend of the water, the float is probably sinking rather than adjusting to new conditions.

### 3. Flow patterns

Nineteen floats were successfully navigated for all or most of the subsurface mission. The ensemble spaghetti diagram for these floats is given in Fig. 5. It is apparent that floats next to the coast moved parallel to the coast, while those farther offshore moved away from the coast, primarily by transport in anticyclonic eddies. A more detailed examination shows that three general patterns are illustrated by the float trajectories: 1) steady poleward flow in the undercurrent, 2) reversing parallel flow that remained near the continental margin, and 3) westward migration, usually in an eddy, in the ocean interior. These will be referred to as California Undercurrent, marginal, and interior patterns.

Most floats exhibited more than one of these flow patterns (Fig. 3a). For example, NPS26 demonstrated marginal reversing flow for the first 35 days, undercurrent flow for the next 50 days and interior flow for the last 40 days of its subsurface mission. To examine the characteristics of each flow type, the trajectories were subjectively broken into segments corresponding to the flow patterns. The general criterion used to distinguish between marginal flow and undercurrent flow was to choose the period when there was continual poleward flow and no subsequent southerly flow. Interior flow was started when the float motion was no longer parallel to the local bathymetry or the float exhibited eddy motion and the water depth exceeded 2000–3000 m. While there was never much ambiguity about the three patterns, the

actual timing of the transition from one to another might be difficult to assign to a particular day. Thus, there may be an error of a few days in choosing the transition from one trajectory pattern to another.

The mean flow for the total float ensemble was directed toward  $310^\circ$  with a vector average speed of  $2.5 \text{ cm s}^{-1}$  and a mean speed of  $8.7 \text{ cm s}^{-1}$  (Table 1). The principal axis of variance was oriented at  $340^\circ$ , with the ellipse of variance having axes of 7.5 and  $6.6 \text{ cm s}^{-1}$ . Examination of the three flow patterns reveals that the segments along the continental margin had the variance oriented with the major axis parallel to the continental margin ( $330^\circ$ ). In the ocean interior, the variance was much more isotropic: the variance axes were 7.7 and  $7.5 \text{ cm s}^{-1}$ .

The remainder of this section will describe the flow patterns observed in the undercurrent, along the continental margin and in the ocean interior.

### *a. California Undercurrent*

The six floats caught in the undercurrent had continuous poleward flow parallel to the coast for distances ranging from 290 to 480 km. The trajectories for these float segments are shown in Fig. 6; Table 2 gives the dates, distance, mean depth, and speed of the six undercurrent float segments.

Four of the floats, NPS 4, 5, 8, and 19 were immediately entrained in the undercurrent. NPS5 (this float has been described in detail by Collins et al. 1996a) remained along the continental margin until near Pt. Saint George ( $41^\circ 50' \text{N}$ ). Then it moved offshore and became entrained in an eddy. During the undercurrent transit, the float generally remained above the 200-m isobath and had a mean speed of  $16.3 \text{ cm s}^{-1}$ . Along the way, the float passed under the active upwelling centers at Pt. Arena and Cape Mendocino. NPS5 represents the shallowest float to date. It oscillated between 115 and 180 dbar with a mean depth of 135 dbar. Our ability to track such a shallow float appears remarkable.

Of the six triads and one pair of RAFOS float deployments, NPS 4 and 8 represent the only instance in which more than one float was entrained in the undercurrent at the time of launching. NPS8 initially traveled faster until  $\sim 39^\circ 30' \text{N}$ , where it slowed down while NPS4 passed inshore of it. At Punta Gorda, the trajectory of NPS4 curved offshore, passing over the Gorda Escarpment and the Mendocino Ridge. NPS4 is the only float to be entrained in the California Current jet flowing offshore at Cape Mendocino. Seven days after NPS4, NPS8 passed northward around Cape Mendocino and its trajectory continued more north-northwest, moving offshore rather than following the bathymetry to the north-northeast. West of Pt. St. George the float became entrained in an eddy that apparently was moving with the undercurrent. Just south of Cape Blanco ( $42^\circ 50' \text{N}$ ), NPS8 left the eddy and began moving westward. The third float of this triad, NPS10, first went southeast and then offshore.

NPS19, launched 25 April 1994, initially settled deep, 420 dbar, but still was carried poleward in the undercurrent, remaining between the 200-m and 1000-m isobath for 50 days, until reaching  $\sim 41^\circ \text{N}$ . There it started gradually moving into deeper water (2000 m) while still moving northward. At about  $41.6^\circ \text{N}$  the float stalled, then began moving westward in an eddy.

Two floats underwent marginal flow before being entrained in the undercurrent. NPS28 remained near the launch site for 25 days before becoming entrained. It then was carried northward to west of Punta Gorda 40 days later. There the float moved offshore and did not curve with the bathymetry north of Cape Mendocino. Instead the float was entrained in an eddy that continued to translate north-northwest for the remainder of the submerged mission.

NPS26 was launched ten days later, 22 August 1994, from a site between Pt. Reyes and Monterey Bay ( $37^\circ 05' \text{N}$ ,  $123^\circ 08' \text{W}$ ). The float moved equatorward along the continental margin for the first 32 days, then swung inshore and began moving poleward in the undercurrent at  $35^\circ 10' \text{N}$ . West of Pt. Arena the float entered an eddy that broke away from the undercurrent. The float was moving westward when it surfaced. This float demonstrated flow continuity from south of Pt. Sur north past Pt. Reyes.

The floats transported in the undercurrent are concentrated in the summer, or wind relaxation, period from July to November, with the exception of NPS19, which was launched in April 1994. NPS5 was launched 7 July 1993, while NPS4 and NPS8 were both launched 3 September 1993. NPS 26 and 28 were launched 10 days and 60 km apart in August 1994.

The vector average flow for these floats was directed toward  $320^\circ$  with onshore and alongshore flows of  $1.8 \pm 1.3$  and  $10.8 \pm 1.4 \text{ cm s}^{-1}$ , respectively. The mean speed,  $11.9 \pm 1.7 \text{ cm s}^{-1}$ , was nearly the same as that observed for interior floats. The principle axis of variance was oriented along  $336^\circ$ , with 5.0 and  $4.7 \text{ cm s}^{-1}$  for the major and minor axes. The range of observed speeds was quite large. NPS5 had a range of daily mean speeds from 4.8 to  $27.9 \text{ cm s}^{-1}$ . Note also that

the shallowest float (135 dbar) had the greatest speed, and the deepest float (420 dbar) the slowest. A linear regression of mean float pressure (dbar) versus mean float speed ( $\text{cm s}^{-1}$ ) for the six floats gives, in this depth range, a depth-related undercurrent speed of  $S(z) = -0.02 \cdot z + 18.4$ , where  $S$  is the speed ( $\text{cm s}^{-1}$ ) and  $z$  is the pressure (dbar). The vertical shear,  $-0.02 \text{ cm s}^{-1} \text{ dbar}^{-1}$ , agrees well with velocity shear estimates of  $-0.016 \text{ cm s}^{-1} \text{ dbar}^{-1}$  from the Pegasus acoustic dropsonde (Rischmiller 1993) but appears to be less than geostrophic shear estimated from the geostrophic velocity sections in Tisch et al. (1992). Collins et al. (1998, manuscript submitted to *Deep-Sea Res.*, hereafter C98) investigate the disparity between geostrophic shear and absolute shear in the undercurrent.

Collins et al. (1996a) noted that undercurrent models predict that float speeds should show a maximum associated with the coastal promontories. To test this, float speed and acceleration were correlated against a number of parameters to examine the speed fluctuations. No significant correlations were found for the float motion with distance offshore, width or divergence of the shelf or slope, and curvature of the coast or shelf margin. A slight trend of decreasing speed as a function of distance offshore was the only possible correlation, but it was not statistically meaningful.

Float speed in the undercurrent did not show any consistent pattern along the coast (Fig. 7) except for the acceleration north of Point Reyes followed by the deceleration south of Pt. Arena. In all cases, the maximum speed was reached south of Pt. Arena, and the floats were decelerating, or had reached a minimum speed, at Pt. Arena. There does not appear to be a preferred motion at either Pt. Reyes or Cape Mendocino. The lowest mean speed was at Pt. Reyes, and the highest at Cape Mendocino, but the latter was influenced by the high speed of NPS5.

Five of the six undercurrent segments ended because the floats became entrained in anticyclonic eddies. The sixth ended when NPS4 became entrained in the offshore-flowing California Current jet at Cape Mendocino. In contrast, entrainment into the undercurrent by the two floats was not by eddy coalescence with the current.

### *b. Marginal flow*

The trajectories of the floats that remained along the continental margin and experienced reversing flow with little net movement are illustrated in Fig. 8. Although the depths of NPS2 and NPS33 were deep, between 600 and 700 dbar, the mean speeds of these two floats were 2.5 and 4.6  $\text{cm s}^{-1}$ , respectively, with most of the movement parallel to the bathymetry.

The four other floats, NPS3, 10, 26, and 28, were between 300 and 350 dbar and experienced extended periods of reversing flow. The mean speeds of these four floats were in the range of 3.1 to 12.3  $\text{cm s}^{-1}$ . NPS3, on a 60-day mission starting 7 July 1993, first moved northwest for 65 km, then onshore, stalled for 10 days and then moved 110 km slowly south for another 20 days. The float then reversed direction, moved north, and surfaced 24 km from the launch point. NPS10, launched 3 September 1993, did a small anticyclonic loop (diameter 20 km) around the launch site during the first 20 days, stalled, then moved south 60 km, stalled again, and then moved into the interior. It spent 50 days along the margin. NPS26 was launched south of the usual launch site and initially moved cyclonically offshore, then southeast to  $35^{\circ}12'N$ . It then curved anticyclonically, entrained in the undercurrent off Cape San Martin ( $35^{\circ}50'N$ ). NPS28, launched off San Francisco, remained in the local area with little movement for 24 days before becoming entrained in the undercurrent.

The floats that encountered reversing marginal flow were launched between year days 190 and 250 (early July to early September), which is representative of the summer season of reduced upwelling and more variable winds. There is probably no statistical significance to this, since most float deployments occurred during the same period. The point to be made, however, is that none of the floats with marginal reversing flow were launched during the winter period, the season ascribed to having reversing flow (Chelton 1984).

By definition, the vector mean speed for marginal floats was low (not significantly different from zero) and the mean speed of 5.0  $\text{cm s}^{-1}$  was only about half that of the other two float classes. The variance ellipse was oriented along  $326^{\circ}$ , with 5.1 and 4.4  $\text{cm s}^{-1}$  for the axes.

The floats undergoing marginal flow were just west of the floats transported in the undercurrent. There appears to be a region directly adjacent to the undercurrent where the flow was polarized alongshore, but with direction and strength variable. This flow also appeared more barotropic with a small vertical velocity gradient.

### *c. Interior flow*

Figure 9 illustrates the interior eastern Pacific trajectories for the 14 floats that were transported away from the continental margin. Seven of the floats moved westward almost immediately after launch, never encountering the

undercurrent. One float exhibiting marginal flow, NPS10, eventually entered the interior. The other five floats were first entrained in the undercurrent. There did not appear to be a pattern to where or when these floats left the undercurrent.


As noted previously, most eddy motion was anticyclonic; only one float (NPS9) never encountered an eddy. Ten of the 14 floats exhibiting interior flow surfaced while still entrained in an eddy. NPS 8 and 19 both entered anticyclonic eddies upon leaving the undercurrent and then apparently left the eddies. NPS8 moved westward, while NPS19 took a large cyclonic curve (130-km diameter) to the north for a period of approximately 25 days followed by 20 days of straight trajectory to the west-northwest. This was the only example of sustained cyclonic flow in any of the interior floats.


The mean speed computed for the interior float segments was  $9.7 \pm 4.1 \text{ cm s}^{-1}$ , while the mean  $u$  and  $v$  velocities were  $-2.0 \pm 1.8$  and  $0.4 \pm 1.6 \text{ cm s}^{-1}$ , respectively. The mean flow direction was  $281^\circ$ , and the vector average speed was  $2 \text{ cm s}^{-1}$ . The direction was primarily due to propagation of the eddy field, which is discussed in [section 5](#). Variability was nearly isotropic, with the axes being  $7.7$  and  $7.4 \text{ cm s}^{-1}$  in length. The predominance of the eddy motion and the distance from the ocean boundary both contribute to the structure of the isotropic variability.

#### *d. Other floats*

Four other float deployments provide further evidence of the barotropic nature of the marginal flow. Three short duration floats (NPS 22, 24, and 30) were launched west of Monterey Bay (centered about  $36^\circ 26' \text{N}$ ,  $122^\circ 55' \text{W}$ ) on 19 May 1994 as part of a coastal tomography experiment ([Benson 1995](#)). The floats, spread between the depths of 300 and 600 dbar, had remarkably similar motion, moving northwest (parallel to the coast), with speeds between  $7.9$  and  $10.2 \text{ cm s}^{-1}$ . Two months earlier in March 1994, a modified RAFOS float launched at  $37^\circ 23' \text{N}$ ,  $122^\circ 41' \text{W}$ , operated between 720 and 840 dbar ([Sanford et al. 1995](#)). Like the tomography floats, it moved northwest with an average speed of  $3.3 \text{ cm s}^{-1}$ .

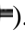
#### *e. Float trajectories and sea surface temperature*

Float trajectories for the first two float triads were superimposed on satellite AVHRR imagery to examine whether there were surface temperature expressions of the motion experienced by the floats. [Lynn and Simpson \(1987\)](#) noted that the California Current regime was dominated by anticyclonic eddies; therefore one might expect to see correspondence between the surface temperature structure and the float subsurface motion. The first triad, NPS 3, 5, and 7, are shown plotted on the SST image for 27 August 1993 ([Fig. 10](#) ). The position of each float for the image day is indicated by an asterisk. On that day NPS3 was at the southern extreme of its trajectory, just starting the return to the north. NPS5 was in an anticyclonic eddy just south of Cape Blanco, where there is a surface signature of cold and warm water deformed anticyclonically. NPS7 was in a warm anticyclonic feature west of San Francisco.

The floats in triad NPS 4, 8, and 10 do not appear to have been in eddies that had surface expressions in the temperature field ([Fig. 11](#) ). NPS4 was moving offshore, along the north side of the Cape Mendocino jet. On the day of the image, 15 November 1993, the float was in a small cyclonic feature that is not apparent in the image. NPS8 had just completed anticyclonic motion in the area south of Cape Blanco. There is no indication of this feature in the SST data. NPS10 was traveling slowly west-northwestward on that day and was located south of another cold jet. The SST data suggest that there may have been anticyclonic motion at the surface.

## **4. Pressure and temperature patterns**

Spectral analyses of the temperature and pressure records were not pursued because of the severe temporal aliasing. The three special tomography floats that sampled temperature and pressure hourly showed mean spectral peaks at 12.6 h for both temperature and pressure ([Benson 1995](#)). These hourly fixes may have aliased the data since the Brunt–Väisälä frequency is about 30 min for the depths of interest. Due to their smaller compressibility, RAFOS floats oscillate faster than the local water column. While not usable for spectral analyses, the daily temperature and pressure records were used for trend recognition and to identify specific events.

The CUC-segment temperature records all showed a northward temperature decrease, while there were mixed results in the pressure records ([Fig. 12](#) ). The two shallowest floats, NPS 4 and 5, sank while traveling northward in the undercurrent but the three floats between 300 and 360 dbar experienced a general rise in depth during the undercurrent transit. The deepest undercurrent float, NPS19, at 430 dbar, underwent a minimal sinking of 0.02 dbar/day, or 1.2 dbar during the 58 days while it was in the undercurrent. NPS19 was identified as a slow sinker due to a leak. Taking this into account, it appears that the floats shallower than 250 dbar underwent a general depth increase, while those deeper than that pressure experienced a general depth decrease while going northward in the undercurrent.

South of Pt. Arena NPS5 slowed down, moved inshore to near the 200-m isobath, rose 20 dbar, and registered a  $0.2^\circ \text{C}$



temperature drop. The float may have been influenced by the deep portion of the upwelling plume observed in the satellite imagery. However, at the stronger Cape Mendocino upwelling site the float accelerated and sank slightly. NPS4 showed no response at Pt. Arena, but rose in cooler water as it left the undercurrent and moved offshore. None of the other floats showed any indication of depth change or water mass change at the major promontories.

[Lynn et al. \(1982\)](#) used California Cooperative Fisheries Investigations (CalCOFI) hydrographic data to demonstrate the alongshore northward decrease in temperature and increase in density at depths above 500 m. Their data show that the alongshore temperature gradient is largest at 300 m, decreasing toward both the surface and depth. The general rising of the floats in this depth range may be a response to the larger temperature gradient.

The two floats that appear to have left eddies before the mission end, NPS 7 and 8, both rose and measured a temperature decrease as they ended anticyclonic motion. This most probably represents the change of water mass and decreased temperatures upon expulsion from the eddies.

The pressure–temperature response of the marginal reversing flow and of the interior eddy segments did not reveal any consistent patterns. Floats in eddies north of Cape Mendocino tended either to have no pressure or temperature trends, or to cool slightly. The two floats, NPS 4 and 31, in large eddies had no gradients of pressure or temperature. The other five eddy segments south of Cape Mendocino revealed an even mix of rising–cooling, sinking–warming, and no pressure or temperature gradients. All gradients were small.

## 5. Eddy characteristics

[Sanderson's \(1995\)](#) least squares technique was applied to estimate the eddy kinematics from the smoothed float segments. The technique allows estimation of both rotational and translational eddy parameters. Float data from 13 floats were used to analyze 12 eddies ([Table 3](#) ). All the eddies were anticyclonic with negative vorticity in the range  $-1.36$  to  $-0.41$  ( $\times 10^{-5} \text{ s}^{-1}$ ). [Figure 13](#)  shows the mean translation vector of each eddy. Adjacent to the undercurrent, eddy motion was  $3.0 \text{ cm s}^{-1}$  in a direction slightly offshore from the poleward bathymetric trend. The average radius was  $32.8 \pm 10.2 \text{ km}$  with a mean rotational period of  $16.5 \pm 5.1$  days. Since there is no way to know the distance from the float to the edge of the eddy, the radii obtained from these float data represent minimums. For eddies away from the continental margin, mean eddy translation was westward with a mean speed of  $1.2 \text{ cm s}^{-1}$ . The float-averaged eddy radius increased to a mean of  $34.8 \pm 21.5 \text{ km}$  with an increased rotational period of  $23.2 \pm 7.4$  days.

NPS31 was the only float clearly in a mesoscale-sized eddy. It had a float motion radius of 71 km and a mean period of 27 days. At the time it surfaced, NPS4 also appeared to be in a mesoscale eddy with radius 67 km and period 35 days. All the other float eddy motion occurred with radii less than 35 km, which is less than the internal Rossby radius, and generally exhibited shorter rotational periods.

Eddy formation apparently occurred within the undercurrent flow region. Neither of the floats entrained in the undercurrent were in eddies at the time of entrainment. NPS 5, 8, 26, and 28 all demonstrated cycloidal motion while still moving northward with the undercurrent. Once developed, the eddy trajectories showed a general westward movement. NPS 6, 11, and 13 illustrated either one eddy splitting or two eddies colliding. Although all three floats began in the same eddy, near the end of the float missions, one float (NPS11) appeared to enter an adjacent eddy while the other two remained in the original feature.

The other floats either entered eddies immediately after being launched (NPS 11, 13, 31) or after leaving the undercurrent and drifting for some time (NPS 6, 7, 10, 14, and 19). Once entrained, most floats remained in eddies for the duration of the submerged drift. The exceptions were floats NPS 7, 8, and 19, which appear to have been ejected from their respective eddies prior to mission end.

## 6. Discussion

### *a. Undercurrent*

The undercurrent and marginal flow segments suggest that the subsurface flow along the northeast Pacific margin can be characterized by a narrow jet, usually located right along the continental slope embedded in a larger region of variable flow that moves parallel to the continental margin. The width of the larger flow regime is not known, but the float data and the analysis of closely spaced Pegasus data ([Rischmiller 1993](#); C98) suggest a width on the order of 100 km. This distance coincides with the location of the dynamic topography trough determined from the CalCOFI hydrographic data ([Schwing et al. 1994](#)).

The embedded undercurrent is a distinct, continuous feature over the distance sampled,  $35^{\circ}$ – $43^{\circ}$ N. The undercurrent has




a sharp offshore boundary, and the undercurrent flow is stronger and has a larger vertical baroclinic shear than the surrounding marginal flow. The vertical current shear between 150 and 600 dbar is  $-0.02 \text{ cm s}^{-1} \text{ dbar}^{-1}$ . The other characteristic of the flow is the development of small eddies that initially move with the flow before breaking away and moving into the ocean interior. Within the present dataset, eddy formation appears to occur all along the sampled region. Some floats were launched into eddies, others reveal eddy development while moving northward.

Annual variability cannot be investigated with these data. However, the present measurements showing a pronounced undercurrent cover the fall and winter periods, the time that [Chelton \(1984\)](#), using geostrophic computations, found little evidence of the undercurrent. Recent analyses of hydrographic data ([Tisch et al. 1992](#)), Pegasus data (C98), and the results of this study suggest that there are significant currents at depth along the continental margin. Perhaps the traditional use of large hydrographic station spacing and the 500-m reference level for dynamic topography previously obscured the existence of the current.

[Hickey \(1979\)](#) suggested a northward weakening of the undercurrent. The floats experienced a general northward temperature decrease, but our results do not support an alongshore speed gradient. Around Cape Mendocino the flow became more variable, but the floats that remained in the undercurrent continued with speeds similar to those farther south. The temperature decrease probably results from the gradual exchange of water in the undercurrent. Cooler water appears to be continually entrained, while the generally warmer undercurrent water is removed through eddy formation and break away.

Off California, surface water is transported offshore in major filaments, or jets, that appear to be anchored at coastal upwelling centers ([Brink and Cowles 1991](#)), and in small filaments, or squirts ([Ramp et al. 1991](#)), as well as in eddies ([Davis 1985](#); SSC). In contrast, offshore transport of subsurface undercurrent water appears to occur primarily through the formation of small subsurface anticyclonic eddies: only one float moved offshore associated with the Cape Mendocino jet, while four others continued northward. As these floats moved offshore, there was no distinct  $T/P$  fluctuation indicating a transition from equatorial to subarctic water. It has not yet been ascertained whether these undercurrent eddies form at fixed geographical locations or more or less randomly along the coast.

South of Point Reyes, in the Gulf of the Farallones, there have been a number of cruises that obtained shipboard acoustic Doppler current profiler (ADCP) measurements that included the continental margin ([Ramp et al. 1995](#); [Parker 1996](#); [Baltz 1997](#); SSC). During 5 of the 14 surveys, strong anticyclonic subsurface eddies with equatorial water cores were found along the continental margin. Unfortunately, most of the surveys did not extend far enough offshore to completely map the undercurrent flow. During 1993 there were three surveys spaced a week apart that demonstrated that the eddies are not stationary. The survey area was not large enough to tag and track each eddy, but it appears that the eddies were moving poleward in the undercurrent.

The moored current meter record from 350 m off Pt. Sur ([Collins et al. 1996b](#)) shows a number of instances of rotary flow reversals with periods on the order of a week or less (their [Fig. 4](#) ). The strength and period of these anticyclonic reversals suggest that they may be eddies moving with the undercurrent.

### *b. Eddies and flow variability*

The small size and anticyclonic rotational bias suggest that undercurrent-spawned eddies are another example of a submesoscale coherent vortex (SCV) formation ([McWilliams 1985](#)). SCVs are small monopoles typified by horizontal scales less than the first baroclinic radius of deformation, an aspect ratio (vertical/horizontal) of the same order as  $f/N$  (the ratio of the Coriolis parameter to the Brunt–Väisälä frequency) ([McWilliams et al. 1983](#)), anticyclonic motion with speeds sometimes exceeding geostrophic balance, and a relative minimum in the vertical density gradient. These eddies appear to have long lives and generally move with the mean regional flow, providing a mechanism for transporting water properties long distances from the source. McWilliams proposed that, although eddy generation had not been observed, a diapycnal mixing process was the most plausible mechanism to consistently produce the anticyclonic SCVs. [D'Asaro \(1988\)](#) proposed another generation mechanism for SCVs found in the Beaufort gyre of the Arctic Ocean. He suggested that anticyclonic eddies are generated in trapped boundary currents when the frictional torque along the continental margin (inshore side of the flow) reduced the potential vorticity to zero. Irregular topography and the frictional effects appear to combine for eddy formation.

The best recognized SCVs are the meddies (Mediterranean eddies) found in the North Atlantic. Several investigators have studied the formation of Mediterranean Water eddies in the North Atlantic ([McDowell and Rossby 1978](#); [Armi et al. 1989](#); [Richardson et al. 1989](#); [Zenk et al. 1992](#); [Pingree and Le Cann 1993](#); [Bower et al. 1997](#)). These eddies provide a mechanism for transporting Mediterranean Water far into the Atlantic interior ([McWilliams 1985](#)). Meddies (McDowell and Rossby) and smeddies (shallow meddies) (Pingree and Le Cann) appear to develop in a region of strong anticyclonic curvature of the bathymetry (viewed in the direction of float motion).

[Bower et al. \(1995, 1997\)](#) suggested that frictional torque was responsible for forming Atlantic meddies at specific locations as the Mediterranean outflow moves along the continental slope. Their results suggest that SCV formation occurs where the topography forms a subsurface promontory. They hypothesize that Cape St. Vincent and Estremadura Promontory are the two principal sites for meddy formation.

Three patterns of eddy motion were observed in the northeastern Pacific, although two of the patterns were each observed by only single floats. NPS4 demonstrated instability along the edge of an offshore flowing filament after it left the undercurrent at Cape Mendocino and moved offshore in a relatively smooth trajectory. Comparison with the satellite AVHRR data for the time suggests that this flow coincides with the surface cold water jet streaming offshore from Cape Mendocino. While moving offshore, the float went through two short meanders, the latter of which was somewhat larger than the former. This float apparently ended its mission in a mesoscale eddy. Clear satellite imagery was not available to determine surface conditions at the time of surfacing.

The second type of motion was associated with mesoscale eddies. NPS31 became entrained in mesoscale anticyclonic motion eight days after launch and remained in the large eddy for the remainder of its mission. This was the only clear example of a float entrained in a mesoscale eddy. Satellite imagery reveals that the eddy had a surface temperature expression, and a RAFOS float at 1580 dbar suggests that the eddy penetrated to at least that depth. The scale of this eddy is similar to scales seen with surface floats ([Brink et al. 1991](#); [Swenson and Niiler 1996](#)).

Ten floats, exhibiting anticyclonic motion with a rotational radius in the range of 15–33 km, appear to be other examples of submesoscale coherent vortices. The vorticity of these SCVs is smaller than the value for typical meddys, but within the range of other SCVs ([D'Asaro et al. 1994](#)). The surrounding vorticity approaches zero giving a vorticity gradient sufficiently strong to inhibit water exchange.

[Huyer et al. \(1998, manuscript submitted to \*Deep-Sea Res.\*\)](#) conducted two large, high-resolution upper-ocean surveys of the California Current region, one in June and the other in August of 1993. Hydrographic parameters were measured in the upper 300 m while the ship was underway through the use of an undulating Seasoar vehicle. Velocity was measured simultaneously using a ship-mounted acoustic Doppler current profiler.

The presence of anticyclonic subsurface eddies were prominent features in each cruise. The “spiciness” ([Flament 1986](#)) was used to show that the eddies contained warm salty water and probably originated in the California Undercurrent at the latitudes of the observations. Huyer et al. estimated that the eddies had formed along the continental margin within the preceding 6–8 months.

The observed eddies were subsurface features with spiciness maximums at 150 m. The two most prominent eddies had radii of 40 and 45 km, the size of the internal Rossby radius, with estimated rotational periods of 9 and 14 days. Both appeared to be in solid body rotation. In addition to the prominent eddies, Huyer et al. measured a number of other eddies, one being the same eddy transporting NPS7. This latter eddy did not have the strong spiciness signature but was still comprised of water saltier and warmer than the surrounding water. There were a number of closely spaced eddies in the vicinity of this eddy. The dimensions of the eddies were similar to the radii of the float motions.

SCV formation is seen both as an eddy transported with the undercurrent (NPS8 and NPS28) and as a feature encountered after the flow has separated from the continental margin (NPS5 and NPS19). The present data combined with ADCP data ([Ramp et al. 1995](#); [Parker 1996](#); [Baltz 1997](#)) suggest that frictional torque is the dominant forcing mechanism for SCVs formed in the undercurrent. Cycloidal motion during eddy formation within the undercurrent might explain why some data suggest that the undercurrent comprises a series of eddies moving poleward rather than of a single coherent current. The present data strongly suggest that the eddy features are created in and transported by the current. In addition to the “eddy zoo” of eastern boundary formed eddies, we suggest that the undercurrent SCVs be referred to as “cuddies” (California Undercurrent eddies).

Once formed, cuddy translation is markedly different than the surface flow. The mixed layer responds to the local wind, and surface drifters demonstrate a generally meandering, but southerly, drift ([Brink et al. 1991](#); [Swenson and Niiler 1996](#)). The small subsurface anticyclonic eddies show a complete decoupling from the surface. All cuddies, once detached from the undercurrent, moved primarily westward. The float trajectories show these eddies being present to at least 131°W, and none of the floats present evidence of eddy decay. Using the observed westward speed of 1.5 cm s<sup>-1</sup>, an eddy could translate about 240 km in six months. Some of the long-duration floats presently deployed may provide more insight on the eddy life spans.

Cuddy westward migration and long duration may explain the offshore subsurface variability in water types.

Temperature–salinity scatterplots of grouped CTD data often reveal increased variability between the 26 and 27 kg m<sup>-3</sup> density anomaly surfaces ([Tisch et al. 1992](#)). In the California Current region off central California, this corresponds to a depth range of about 150–600 m. The variability may exist because the undercurrent anticyclonic eddies allow the equatorial

Pacific water signature to remain intact for the lifetime of the eddies. This provides a mechanism for delivering the equatorial Pacific water offshore and could explain why the  $T-S$  variability remains strong and why this water is often found embedded in southerly flowing California Current water.

The occurrence of undercurrent eddies transporting equatorial Pacific water into the eastern Pacific interior in a manner similar to meddy transport in the Atlantic suggests that this is an important mechanism wherever midlatitude eastern boundary currents exist. Lagrangian studies in the south Atlantic, the south Pacific, and Indian Oceans will very likely encounter similar anticyclonic subsurface eddies associated with eastern boundary currents.

## 7. Conclusions

The RAFOS dataset reveals two distinct features of the undercurrent flow: the flow continuity over a four-degree latitudinal range, and the distinct differences between surface and 300-m flow in the interior eastern Pacific. The observed undercurrent flow continuity was anticipated, and the present floats provide new data for examining the flow speed along a curving continental margin. The measured speeds do not conform to existing theoretical models of subsurface flow. Neither the presence of SCV eddies nor that of a mean westward interior flow were anticipated at the start of this program. To further verify the presence of SCV eddies, the historical data need to be examined for the existence of distinct subsurface signatures of equatorial water embedded in the subarctic waters of the offshore California Current.

## Acknowledgments

We thank Tarry Rago, who has been directly involved with all aspects of this program. Kirk Kingsbury, NCEL pressure facility director and operator, repeatedly went out of his way to ensure that ballasting went smoothly and successfully. Mike Cook is thanked for his MATLAB tutoring. N.G. and C.A.C. thank Jeff Paduan for many beneficial discussions. Frank Schwing first suggested the name “cuddy.” The suggestions of the two reviewers substantially improved this manuscript. We acknowledge support from the Naval Postgraduate School, the Oceanographer of the Navy, and the Office of Naval Research.

---

## REFERENCES

- Armi, L., D. Hebert, N. Oakey, J. Price, P. L. Richardson, T. Rossby, and B. Ruddick, 1989: Two years in the life of a Mediterranean salt lens. *J. Phys. Oceanogr.*, **19**, 354–370. [Find this article online](#)
- Baltz, K. A., 1997: Ten years of hydrographic variability off central California during the upwelling season. M.S. thesis, Department of Oceanography, Naval Postgraduate School, Monterey, CA, 319 pp. [Available from Department of Oceanography, Naval Postgraduate School, 833 Dyer Rd., RM 328, Monterey, CA 93943.]
- Benson, K. R., 1995: High frequency subsurface Lagrangian measurements in the California Current with RAFOS floats. M.S. thesis, Department of Oceanography, Naval Postgraduate School, Monterey, CA, 88 pp. [Available from Department of Oceanography, Naval Postgraduate School, 833 Dyer Rd., RM 328, Monterey, CA 93943.]
- Bower, A. S., 1994: *RAFOS Float Technology Workshop Proceedings*. Woods Hole, MA, Woods Hole Oceanographic Institution, 115 pp..
- , L. Armi, and I. Ambar, 1995: Direct evidence of meddy formation off the southwestern coast of Portugal. *Deep-Sea Res.*, **42**, 1621–1630..
- , —, and —, 1997: Lagrangian observations of Meddy formation during a Mediterranean Undercurrent seeding experiment. *J. Phys. Oceanogr.*, **27**, 2545–2575. [Find this article online](#)
- Brink, K. H., and T. J. Cowles, 1991: The Coastal Transition Zone Program. *J. Geophys. Res.*, **96** (C8), 14 637–14 647..
- , R. C. Beardsley, P. P. Niiler, M. Abbott, A. Huyer, S. Ramp, T. Stanton, and D. Stuart, 1991: Statistical properties of near-surface flow in the California coastal transition zone. *J. Geophys. Res.*, **96** (C8), 14 693–14 706..
- Chelton, D. B., 1984: Seasonal variability of alongshore geostrophic velocity off central California. *J. Geophys. Res.*, **89**, 3473–3486..
- Collins, C. A., N. Garfield, R. G. Paquette, and E. Carter, 1996a: Lagrangian measurement of subsurface poleward flow between 38°N and 43°N along the West Coast of the United States during summer, 1993. *Geophys Res Lett.*, **23**, 2461–2464..
- , R. G. Paquette, and S. R. Ramp, 1996b: Annual variability of ocean currents at 350m-depth over the continental slope off Point Sur, California. *CalCOFI Reports*, Vol. 37, 1–7. [Available from Southwest Fisheries Science Center, National Marine Fisheries Service,

— ,N. Garfield, T. A. Rago, F. W. Rischmiller, and E. Carter, 1998: Mean structure of the inshore countercurrent and California Undercurrent off Point Sur, California. *Deep-Sea Res.*, in press..

D'Asaro, E. A., 1988: Generation of submesoscale vortices: A new mechanism. *J. Geophys. Res.*, **93** (C6), 6670–6694..

— ,S. Walker, and E. T. Baker, 1994: Structure of two hydrothermal megaplumes. *J. Geophys. Res.*, **99** (C10), 20 361–20 373..

Davis, R. E., 1985: Drifter observations of coastal surface currents during CODE: Method and descriptive view. *J. Geophys. Res.*, **90**, 4741–4755..

— ,1991: Observing the general circulation with floats. *Deep-Sea Res.*, **38**(Suppl. 1), S531–S571..

Flament, P., 1986: Finestructure and subduction associated with upwelling filaments. Ph.D. dissertation, University of California, San Diego, 142 pp. [Available from Scripps Institute of Oceanography, University of California, La Jolla, CA 92093-0230.].

Freeland, H. J., W. R. Crawford, and R. E. Thomson, 1984: Currents along the Pacific coast of Canada. *Atmos.-Ocean*, **22**, 151–172..

Goodman, L., and E. R. Levine, 1990: Vertical motion of neutrally buoyant floats. *J. Atmos. Oceanic Technol.*, **7**, 38–49..

Hickey, B. M., 1979: The California Current System—Hypotheses and facts. *Progress in Oceanography*, Vol. 12, Pergamon, 259–284..

Huyer, A., P. M. Kosro, S. Lentz, and R. C. Beardsley, 1989: Poleward flow in the California Current System. *Poleward Flows along Eastern Oceanic Boundaries*, Coastal and Estuarine Studies No. 34, E. Neshyba, et al., Eds., Springer-Verlag, 142–156..

— ,J. A. Barth, P. M. Kosro, R. K. Shearman, and R. L. Smith, 1998: Upper-ocean water mass characteristics of the California Current, summer 1993. *Deep-Sea Res.*, in press..

Johnson, R. H., and R. A. Norris, 1968: Geographic variation of sofar speed and axis depth in the Pacific Ocean. *J. Geophys. Res.*, **73**(14), 4695–4700..

Largier, J. L., B. A. Magnell, and C. D. Winet, 1993: Subtidal circulation over the Northern California Shelf. *J. Geophys. Res.*, **98** (C10), 18 147–18 179..

Lynn, R. J., and J. J. Simpson, 1987: The California Current System: The seasonal variability of its physical characteristics. *J. Geophys. Res.*, **92**, 12 947–12 966..

— ,K. A. Bliss, and L. E. Eber, 1982: Vertical and horizontal distributions of seasonal mean temperature, salinity, sigma-T, stability, dynamic height, oxygen, and oxygen saturation in the California Current, 1950–1978. *CalCOFi Atlas*, No. 50, Southwest Fisheries Science Center. [Available from Southwest Fisheries Science Center, National Marine Fisheries Service, FSWC1, 8604 La Jolla Shore Dr., La Jolla, CA 92038.].

McDowell, S. E., and H. T. Rossby, 1978: Mediterranean Water: An intense mesoscale eddy off the Bahamas. *Science*, **202**, 1085–1087..

McWilliams, J. C., 1985: Submesoscale, coherent vortices in the ocean. *Rev. Geophys.*, **23**, 165–182..

— ,E. D. Brown, H. L. Bryden, C. C. Ebbesmeyer, B. A. Elliott, R. H. Heinmiller, B. Lien Hua, K. D. Leaman, E. J. Lindstrom, J. R. Luyten, S. E. McDowell, W. B. Owens, H. Perkins, J. F. Price, L. Regier, S. C. Riser, H. T. Rossby, T. B. Sanford, C. Y. Shen, B. A. Taft, and J. C. van Leer, 1983: The local dynamics of eddies in the Western North Atlantic. *Eddies in Marine Science*, A. R. Robinson, Ed., Springer-Verlag, 92–113..

Mooers, C. N. K., 1989: Workshop Summary: Poleward flow—Observational and theoretical issues. *Poleward Flows along Eastern Oceanic Boundaries*, Coastal and Estuarine Studies No. 34, E. Neshyba, et al., Eds., Springer-Verlag, 3–16..

Noble, M., R. C. Beardsley, J. V. Gardner, and R. L. Smith, 1987: Observations of subtidal currents over the northern California continental slope and adjacent basin: Some evidence for local wind forcing. *J. Geophys. Res.*, **92**(C2), 1709–1720..

Paduan, J. D., and P. P. Niiler, 1993: Structure of velocity and temperature in the northeast Pacific as measured with Lagrangian drifters in fall 1987. *J. Phys. Oceanogr.*, **23**, 585–600.. [Find this article online](#)

Paquette, R. G., 1996: *RAFOS Float Manual*. Naval Postgraduate School, Monterey, CA., 44 pp. [Available from Department of Oceanography, Naval Postgraduate School, 833 Dyer Rd., RM 328, Monterey, CA 93943.].

Parker, H. A., 1996: Variations in coastal circulation off central California, Spring–Summer of 1993, 1994, and 1995. M.S. thesis, Department of Oceanography, Naval Postgraduate School, Monterey, CA, 71 pp. [Available from Department of Oceanography, Naval

- Pingree, R. D., and B. Le Cann, 1993: A shallow meddy (a Smeddy) from the secondary Mediterranean salinity maximum. *J. Geophys. Res.*, **98**, 20 169–20 185..
- Poulain, P.-M., and P. P. Niiler, 1989: Statistical analysis of the surface circulation in the California Current System using satellite-tracked drifters. *J. Phys. Oceanogr.*, **19**, 1588–1603.. [Find this article online](#)
- , A. Warn-Varnas, and P. P. Niiler, 1996: Near-surface circulation of the Nordic seas as measured by Lagrangian drifters. *J. Geophys. Res.*, **101**(C8), 18 237–18 258..
- Ramp, S. R., P. F. Jessen, K. H. Brink, P. P. Niiler, F. L. Daggett, and J. S. Best, 1991: The physical structure of cold filaments near Point Arena, California, during June 1987. *J. Geophys. Res.*, **96**(C8), 14 859–14 884..
- , N. Garfield, C. A. Collins, L. K. Rosenfeld, and F. B. Schwing, 1995: Circulation studies over the continental shelf and slope near the Farallon Islands, CA. Naval Postgraduate School Tech. Rep. NPS-OC-95-004, 22 pp. [Available from Department of Oceanography, Naval Postgraduate School, 833 Dyer Rd., RM 328, Monterey, CA 93943.].
- Reid, J. L., 1962: Measurements of the California Countercurrent at a depth of 250 meters. *J. Mar. Res.*, **20**, 134–137..
- Richardson, P. L., D. Walsh, L. Armi, M. Schroeder, and J. F. Price, 1989: Tracking three meddies with SOFAR floats. *J. Phys. Oceanogr.*, **19**, 371–383.. [Find this article online](#)
- Rischmiller, F. W., 1993: Variability of the California Current System off Point Sur, California, from April 1988 to December 1990. M.S. thesis, Department of Oceanography, Naval Postgraduate School, Monterey, CA, 159 pp. [Available from Department of Oceanography, Naval Postgraduate School, 833 Dyer Rd., RM 328, Monterey, CA 93943.].
- Rosenfeld, L. K., F. B. Schwing, N. Garfield, and D. E. Tracy, 1994: Bifurcated flow from an upwelling center: A cold water source from Monterey Bay. *Contin. Shelf Res.*, **14**, 931–964..
- Rosby, H. T., E. R. Levine, and D. N. Connors, 1985: The Isopycnal Swallow Float—A simple device for tracking water parcels in the ocean. *Progress in Oceanography*, Vol. 14, Pergamon, 511–525..
- Rosby, T., D. Dorson, and J. Fontaine, 1986: The RAFOS System. *J. Atmos. Oceanic Technol.*, **3**, 672–679..
- Sanderson, B. G., 1995: Structure of an eddy measured with drifters. *J. Geophys. Res.*, **100**(C4), 6761–6776..
- Sanford, T. B., R. G. Deaver, and J. H. Dunlap, 1995: Barotropic ocean velocity observations from an Electric Field Float, a modified RAFOS float. *Proc. IEEE Fifth Working Conf. on Current Measurement*, S. P. Anderson, G. F. Appell, A. J. Williams III, Eds. New York, NY, IEEE, 163–168..
- Schwing, F. B., D. M. Husby, N. Garfield, and D. E. Tracy, 1991: Mesoscale oceanic response to wind events off central California in Spring 1989: CTD surveys and AVHRR imagery. *CalCOFI Reports*, Vol. **32**, 47–62. [Available from Southwest Fisheries Science Center, National Marine Fisheries Service, FSWC1, 8604 La Jolla Shore Dr., La Jolla, CA 92038.].
- Smith, R. L., S. D. Pierce, J. A. Barth, P. M. Kosro, and C. Wilson, 1996: Extensive observations of the poleward undercurrent along the continental margin off California, Oregon and Washington. Abstract only. *Eos., Trans. Amer. Geophys. Union*, **77**(3), (Suppl.), OS131..
- Steger, J., F. Schwing, C. A. Collins, L. Rosenfeld, N. Garfield, and E. Gezgin, 1998: Circulation and water masses in the Gulf of the Farallones. *Deep-Sea Res.*, in press..
- Stevenson, M. R., J. G. Pattullo, and B. Wyatt, 1969: Subsurface currents off the Oregon coast as measured by Parachute Drogues. *Deep-Sea Res.*, **16**, 449–461..
- Swenson, M. S., and P. P. Niiler, 1996: Statistical analysis of the surface circulation of the California Current. *J. Geophys. Res.*, **101** (C10), 22 631–22 645..
- Swift, D. D., and S. C. Riser, 1994: RAFOS Floats: Defining and targeting surfaces of neutral buoyancy. *J. Atmos. Oceanic Technol.*, **11**, 1079–1092..
- Taylor, G. I., 1921: Diffusion by continuous movements. *Proc. London Math. Soc.*, **20**, 196–212..
- Thomson, R. E., P. H. LeBlond, and W. J. Emery, 1990: Analysis of deep-drogued satellite-tracked drifter measurements in the northeast Pacific. *Atmos.–Ocean*, **24**, 409–443..
- Tisch, T. D., S. R. Ramp, and C. A. Collins, 1992: Observations of the geostrophic current and water mass characteristics off Point Sur,

Wooster, W. S., and J. H. Jones, 1970: California Undercurrent of northern Baja California. *J. Mar. Res.*, **28**, 253–260..

Zenk, W., K. Schultz-Tokos, and O. Boebel, 1992: New observations of meddy movement south of the Tejo Plateau. *Geophys. Res. Lett.*, **19**, 2389–2392..

---

## APPENDIX

### 8. Float Statistics

The mean currents in the interior and the principle axis of variance found from the RAFOS floats are different from results of surface drifters from this region. [Swenson and Niiler \(1996\)](#) summarize most surface Lagrangian measurements obtained between 1985 and 1990. In their most northerly box (40°N, 125°W) they show (their [Fig. 7](#)) a mean south-southwest flow with a vector speed of about  $18 \text{ cm s}^{-1}$ . They also report large asymmetry to the variance axes. The principle axis is oriented at 40°. That contrasts with the subsurface results found here, a mean flow directed to 310° and a vector mean speed of  $2.8 \text{ cm s}^{-1}$ . One variance axis was oriented at 340°, with little asymmetry to the variance magnitude. [Davis \(1985\)](#) noted that the offshore-directed mean is not necessarily an indication of divergent flow, but could be the result of the existence of the boundary, which inhibits onshore flow.

Results from single- and two-particle statistical analyses are presented. The small size of the dataset and the range in pressure mean that these estimates have large uncertainties. These preliminary results are described here in order to allow comparison with other published results.

#### *a. Diffusivity and dispersion*

For purposes of computing both Eulerian and Lagrangian statistics, NPS22 was not used because the record length was less than 20 days. The number of degrees of freedom for statistical analyses was increased by creating “pseudo” floats. Every 10 days, the position of a float was used as the starting point for a “new” pseudofloat that then traveled as the parent float. In this manner, a float with a 95-day record, for example, would be used to create a set of seven floats, the original float record of 95 days plus six pseudofloats of 85, 75, . . . , 35 days. Minimum record length for the pseudofloats was 20 days. In this way the number of “floats” available for statistical analyses was increased from 19 to 141. Each float was also separated into groups corresponding to the three patterns of flow with the statistics then determined, again creating pseudofloats by restarting each float at 10-day intervals. Thus, the sum of the pseudofloats for the segments does not total the 141 pseudofloats for the entire record. The statistics were also computed with the coordinate system rotated 32° counterclockwise, parallel to the coast so that velocity components representing onshore ( $u_p$ ) and alongshore ( $\mathbf{v}_p$ ) flow could also be determined. Estimated float statistics for the entire float ensemble and for the three patterns of float motion include mean speed, velocity, and velocity variability as well as the Lagrangian velocity correlation scales.

Our data cannot resolve interannual or annual variability, but these statistics can describe the character of the observed patterns.

#### 1) ARRAY BIAS

Our project design of deploying the floats near the shore complicates estimating both Eulerian and Lagrangian statistics. [Swenson and Niiler \(1996\)](#) discuss biasing problems present in determining Eulerian statistics when, as in the present study, the deployment distribution is concentrated into one region. Floats originating from the eastern margin reach the interior from only one direction. There is no contribution of floats arriving from the west. Spatial variability in the small-scale, eddy dispersive field will bias Eulerian averages, and statistical reliability will be reduced in regions of high velocity since floats do not remain in those areas. Floats constrained to a depth, whether surface or subsurface, do not sample convergence effects. In addition to those problems, our RAFOS array did not sample at a single depth; float depths ranged from 135 to 650 dbar. Vertical shear is not estimated, but is treated as horizontal shear. The noted depth dependence of the undercurrent speed emphasizes this last problem. Finally, the small size of the present dataset does not allow robust statistical confidence. Despite all these problems and the large uncertainty to the computed values, the comparison with other published values suggests that the results are indicative of the subsurface diffusion.

#### 2) SINGLE PARTICLE STATISTICS

Single particle statistical methods ([Taylor 1921](#)) have been extended for oceanographic application. We follow the

formulations that appear in the recent work of, among others, [Poulain and Niiler \(1989\)](#), [Thomson et al. \(1990\)](#), [Brink et al. \(1991\)](#), [Paduan and Niiler \(1993\)](#), and [Poulain et al. \(1996\)](#). Since a large number of independent observations are necessary to recover reliable statistics, the practice of creating a larger set of floats by starting pseudo floats from each float after a set time was used.

Decorrelation time and space scales, flow polarization, and the rate of mixing, can be estimated from the flow variance, which is inferred from the sample Lagrangian autocovariance function

$$R_{ij}(\tau, T) = \frac{1}{T} \int_0^T u'_i(t) u'_j(t + \tau) dt, \quad (\text{A1})$$

where  $u' = u - u_{\text{mean}}$  is the perturbation velocity at each time,  $\tau$  is the time lag, and  $T$  is the length of the time series ([Paduan and Niiler 1993](#)). The autocorrelation functions are obtained by normalizing the covariance functions. The mean float polarization, or sense of rotation, is defined as

$$J(\tau) = \int_0^\tau (R_{uv}(\tau') - R_{vu}(\tau')) d\tau', \quad (\text{A2})$$

where  $R_{ij}$  is cross correlation ([Poulain and Niiler 1989](#)). A positive  $j$  is dominated by cyclonic rotation, while a negative  $j$  indicates domination by anticyclonic rotation. In the mean the flow is anticyclonic, most strongly so in the interior flow where the motion is dominated by the eddy field.

[Poulain and Niiler \(1989\)](#) define the Lagrangian integral time  $T^L$  and space  $L^L$  scales as the time and distance over which a drifter remembers its path

$$T_i^L \equiv \frac{1}{\langle u_i'^2 \rangle_L} \int_0^t R_{ii}(\tau) d\tau \quad (\text{A3})$$

and

$$L_i^L \equiv \frac{1}{[\langle u_i'^2 \rangle_L]^{1/2}} \int_0^t R_{ii}(\tau) d\tau = [\langle u_i'^2 \rangle_L]^{1/2} T_i^L, \quad (\text{A4})$$

where  $\langle \rangle_L$  represents the Lagrangian average. The autocorrelation functions are time dependent, and the usual practice for estimating the time and space scales is to integrate the autocorrelation function from zero to the time of the first zero crossing. Estimates of the Lagrangian space and Eulerian time scales based on the Lagrangian autocorrelation functions for these float trajectories are given in [Table A1](#). The Lagrangian time scale varied between 2.7 days in the undercurrent to 5.6 days for floats showing reversing flow along the continental margin. A 5-day decorrelation time indicates that creating the pseudofloats by restarting the float trajectories every 10 days did not introduce a bias.

The single particle diffusivities represent the time rate of change of dispersion about the mean trajectory, or the rate at which the envelope of float paths diverges from the mean. By design, the floats were deployed in a region with asymmetric velocity patterns. The diffusivities for the undercurrent and marginal flow cases are not meaningful because those flows are constrained by the boundary. The diffusivity is meaningful for the interior floats. The diffusivity was estimated from the Lagrangian autocovariance function ([Paduan and Niiler 1993](#)) as

$$K_{ii}(t) = \int_0^t R_{ii}(\tau) d\tau. \quad (\text{A5})$$

Here  $K_{ii}(t)$  should approach asymptotic values,  $K_{\infty}$ , for long timescales ([Davis 1991](#)). The diffusivity given in [Table A1](#) is an estimate of  $K_{\infty}$ . It was reached at a time interval longer than the estimated integral timescale. The cross-shore

diffusion,  $2015 \text{ m}^2 \text{ s}^{-1}$  was slightly larger than the alongshore diffusion,  $1788 \text{ m}^2 \text{ s}^{-1}$ . Subsurface diffusion does not show a significant bias in either direction, probably due to the eddy field dominance.

The single particle diffusivities determined for the floats in the Pacific interior can be compared with other estimates (Table A2). Thomson et al. (1990) analyzed the trajectories of a series of surface drifters that were drogued at 100 to 120 m. Their study was in the eastern Pacific west of Queen Charlotte Island, and the mean trajectory of their floats was eastward. Their mean diffusivities were about the same as those found in the present study. The major difference is that their  $K_{\text{uv}}$  component was larger than the  $K_{\text{uu}}$  component, while the present result shows less directional variability.

The diffusivities at 300-m depth from the RAFOS floats can also be contrasted with surface float single particle statistics derived from floats that traversed the same region. Brink et al. (1991) reported surface diffusivities that were larger than the subsurface values by a factor of 2 to 3. Unlike the present study, they found  $K_{\text{uu}}$  to be larger than  $K_{\text{uv}}$  by a factor of 3.5.

Results from drifter studies to the north, off Vancouver Island (Paduan and Niiler 1993) and south of Pt. Conception (Poulain and Niiler 1989), had diffusivity values closer to the present study, but, like Thomson et al. (1990), with  $K_{\text{uv}}$  larger than  $K_{\text{uu}}$ . Swenson and Niiler (1996) demonstrated the areal variability of single particle diffusion and give a range of 2000–5500 and 1100–8700  $\text{m}^2 \text{s}^{-1}$  for the zonal and meridional diffusivities. They did not calculate values for the region represented in the present study.

The decorrelation time and length scales for both surface and subsurface measurements all fall within a similar range of 2–5 days and 15–40 km.

### 3) TWO-PARTICLE STATISTICS

Triads of floats were released in order to estimate directly the dispersion from spreading particles. The three triads and the float pairs NPS 9 and 14 and NPS 28 and 33 provide 11 particle-pair measurements originating from the launch point west of San Francisco. The estimate from such a small number of pairs is extremely noisy. Many more float returns will be necessary before statistically robust estimates will be possible. With that understanding, we present these preliminary results for comparison with the single particle estimates.

The rate at which two particles separate is the eddy diffusivity for the time-dependent spreading of particles (Davis 1985). In a manner similar to the single particle diffusivity, the particle-pair diffusivity can be expressed as

$$\alpha^{ij} = \frac{1}{4} \frac{d}{dt} \left( \frac{1}{N} \sum s^{i'} s^{j'} \right), \quad (\text{A6})$$

where  $s^{i'}$  is the deviation of any particle pair from the mean separation of many pairs at that time step ( $s^{i'} = s^i - \bar{s}$ ). Particle-pair dispersion was estimated for the triad deployments released from the primary launch site.

After an initial 3-day period of equal growth, the alongshore component of variance continues to grow while the cross-shore component begins to oscillate. This demonstrates the anisotropic nature of the flow; westward moving floats encountered slow moving eddies, while floats in the undercurrent continued to move poleward. Northward variance is larger because of the spreading between floats in the undercurrent and floats entering the interior. Eastward variance remained smaller because there are no currents producing similar eastward shear.

The particle-pair diffusivities are extremely noisy, showing oscillatory behavior starting with day 10 and increasing in amplitude for both northward and eastward components. The development of the oscillatory behavior is most probably related to an increasing number of floats becoming entrained in eddies after leaving the undercurrent. In the mean, the alongshore diffusivity is a factor of 6 greater than the cross-shore diffusivity.

Our computed two-particle statistics are extremely noisy. In part this is due to only having a limited number of floats. It is also due to the float mission length being shorter than the lifespan of the SCV eddies. The eddies appear to have limited diffusion during their existences, so the particle pair variance is a reflection of the eddy rotation and slow drift rather than of particle diffusion in a more homogeneous fluid.

---

## Tables

Table 1. Float velocity and speed statistics.



Type of flow	Number of floats	Pseudofloat	$U$ mean and std dev (cm s <sup>-1</sup> )	$V$ mean and std dev (cm s <sup>-1</sup> )	Mean speed and std dev (cm s <sup>-1</sup> )
(a) determined from apportioning the floats into the different types of observed flow					
All	19	141	-1.7 ± 1.8	0.9 ± 2.6	8.7 ± 4.1
Undercurrent	6	14	-4.1 ± 1.1	1.0 ± 1.6	11.0 ± 3.7
Interior	6	38	-0.02 ± 1.5	-1.0 ± 2.3	5.0 ± 1.8
Interior	13	75	-2.0 ± 1.8	0.4 ± 1.6	9.7 ± 4.4
(b) in a coordinate system rotated counterclockwise 32° to alongshore and across-shore axes) from apportioning the floats into the different types of observed flow					
			$U'$ mean and std dev	$V'$ mean and std dev	Mean speed and std dev
All	19	141	-1.0 ± 1.7	1.7 ± 2.7	8.7 ± 4.1
Undercurrent	6	14	1.8 ± 1.3	1.0 ± 1.4	11.0 ± 3.7
Interior	6	38	-0.6 ± 0.5	-0.8 ± 2.6	5.0 ± 1.8
Interior	13	75	-1.2 ± 1.9	1.4 ± 1.4	9.7 ± 4.4

Click on thumbnail for full-sized image.

Table 2. The transit dates, alongshore distance, and mean and standard deviation of the depth and speed for the six float segments within the undercurrent.

Float	Start date	Days in current	Alongshore distance (km)	Depth (flm)	Speed (cm s <sup>-1</sup> )
4	5 Sep 1993	27	286	242 ± 4	13.0 ± 5.1
5	8 Jul 1993	34	435	135 ± 14	16.0 ± 5.2
8	5 Sep 1993	43	410	302 ± 12	11.4 ± 5.2
19	20 Aug 1994	95	454	429 ± 7	10.1 ± 4.4
26	28 Sep 1994	50	480	314 ± 7	12.5 ± 3.6
28	6 Sep 1994	50	497	357 ± 9	11.4 ± 3.8

Click on thumbnail for full-sized image.

Table 3. Eddy kinematics for strongly rotational float segments in both the undercurrent and the ocean interior: %  $U$ , %  $V$  are the percentages of the  $U$  and  $V$  velocity components, respectively, accounted for by the combination of rotation and eddy translation.

Float	Start date	Latitude (°N)	Longitude (°W)	$u, v$ (cm s <sup>-1</sup> )	Radius (km)	Period (days)	Vorticity ( $10^{-4}$ s <sup>-1</sup> )	% $U$	% $V$
4	4 Dec 1993	39.1	128.3	-2.15 ± 0.19	0.68	18.7	-0.41	99.8	98.9
5	12 Aug 1993	42.2	125.3	-0.83 ± 0.38	1.74	10.8	-1.36	90.1	88.9
6, 11, 13	3 Dec 1993	37.8	126.6	-0.86 ± 0.72	2.68	24.5	-0.61	83.6	72.8
7	10 Jan 1994	37.5	125.5	-0.98 ± 0.87	1.80	17.7	-0.84	96.9	97.4
11	27 Jul 1993	37.2	125.4	-2.40 ± 0.94	2.31	11.9	-1.23	96.4	94.4
14	19 Oct 1993	41.6	125.0	-0.61 ± 0.95	2.95	21.0	-0.71	94.9	92.5
19	16 Dec 1993	38.2	125.7	-1.22 ± 0.96	1.71	22.8	-0.64	94.9	94.3
16	30 Jan 1994	38.2	124.6	-0.99 ± 0.47	2.65	24.2	-0.61	97.5	98.5
19	7 Jan 1994	41.6	126.4	-2.25 ± 0.68	26.2	16.6	-0.90	94.9	75.6
26	14 Nov 1994	39.0	124.3	-4.71 ± 1.21	27.9	13.7	-1.07	84.0	83.1
28	22 Nov 1994	41.1	125.3	-2.40 ± 1.30	33.8	15.4	-0.93	94.9	84.8
31	31 Aug 1994	38.7	126.3	-1.50 ± 1.53	73.2	27.3	-0.55	99.0	98.5

Click on thumbnail for full-sized image.

Table A1. Estimation of the Lagrangian time, space, and diffusion scales.

Type	Number of floats	Timescales		Length scales		Diffusivity		
		$U$ (days)	$V$ (days)	$U$ (km)	$V$ (km)	$K_{\text{eff}}$ (m <sup>2</sup> s <sup>-1</sup> )	$K_{\text{eff}}$ (m <sup>2</sup> s <sup>-1</sup> )	
(a) from the Lagrangian autocorrelation function								
All fls	19	141	4.4 ± 1.7	4.6 ± 2.0	21.2 ± 15.4	23.1 ± 13.0	1421 ± 1750	1476 ± 1590
Undercurrent	6	14	2.7 ± 0.4	2.9 ± 0.7	9.5 ± 3.4	11.4 ± 3.4	415 ± 237	480 ± 165
Interior	13	75	4.4 ± 1.8	4.0 ± 1.3	25.5 ± 15.0	23.1 ± 15.1	1965 ± 2095	1831 ± 2026
Interior	6	38	5.0 ± 1.2	5.6 ± 2.2	12.6 ± 3.6	18.4 ± 9.1	367 ± 280	629 ± 360
(b) from the Lagrangian autocorrelation function with the coordinate system rotated 32° counterclockwise								
			$U'$	$V'$				
All fls	19	141	4.4 ± 1.7	4.6 ± 2.0	21.2 ± 15.4	23.1 ± 13.0	1421 ± 1750	1476 ± 1590
Undercurrent	6	14	2.7 ± 0.5	2.7 ± 0.6	9.6 ± 3.3	10.9 ± 3.2	409 ± 269	462 ± 181
Interior	13	75	4.4 ± 1.8	4.0 ± 1.5	25.8 ± 15.7	23.1 ± 14.6	2016 ± 2103	1789 ± 1990
Interior	6	38	4.8 ± 1.2	5.8 ± 2.3	12.3 ± 3.7	19.0 ± 9.0	358 ± 233	644 ± 411

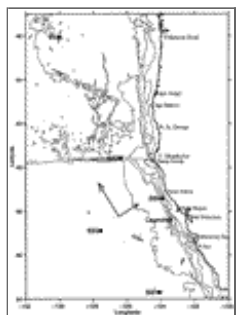
Click on thumbnail for full-sized image.

Table A2. Comparison of interior single particle statistics with other eastern Pacific Lagrangian estimates.

Author	Diffusivity		Timescales		Length scales	
	$K_{\text{eff}}$ (m <sup>2</sup> s <sup>-1</sup> )	$K_{\text{eff}}$ (m <sup>2</sup> s <sup>-1</sup> )	$U$ (days)	$V$ (days)	$U$ (km)	$V$ (km)
present study	1970	1830	4.4	4.0	25	23
	1700	2200	2.6	2.7	20	23
Pudun and Miller (1989)	3400	4300	4.2	4.7	40	48
	8620	2430	3.3	0.9		
Pudun and Miller (1993)	835	1234	2.8	3.8	13.9	22.0

Click on thumbnail for full-sized image.

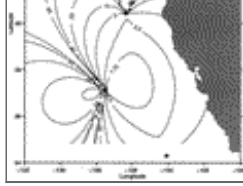
## Figures



Click on thumbnail for full-sized image.

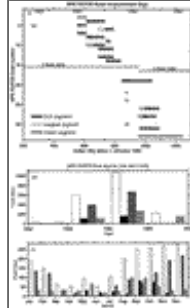
Fig. 1. Northeast Pacific between southern California and Washington locating the four NPS sound sources (SS1 to SS4) and the NOAA PMEL sound source (V1). The isobaths for 200, 1000, 2000, 3000, and 4000 m are contoured. The primary launch site is indicated by the open circle. The two arrows show the orientation for rotating the float velocity into along- and across-shore directions





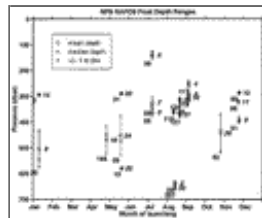
[Click on thumbnail for full-sized image.](#)

Fig. 2. Dilution of precision (DOP) for the eastern Pacific computed for the geometry of the three southern sound sources (SS 1–3). Units are kilometers. Note that the northern sources were used for navigating floats north of Cape Mendocino, not the sources diagramed in this figure.



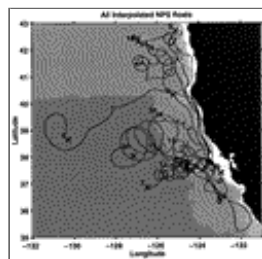
[Click on thumbnail for full-sized image.](#)

Fig. 3. (a) Deployment schedule for the 20 floats used in this study. The shading separates the float days into the three types of observed motion. Black are float days in the California Undercurrent, dark gray are float days in the interior region, and light gray are float days for reversing marginal flow. The white region in NPS6 represents period of unknown position. (b) Frequency distribution of the number of float daily observations as a function of year and (c) month. White bars in b and c indicate the total float days for all floats.



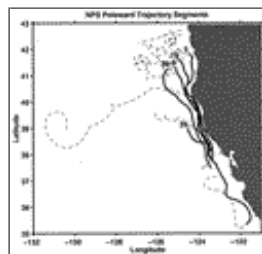
[Click on thumbnail for full-sized image.](#)

Fig. 4. Depth range (mean, median, and standard deviation) of the NPS RAFOS floats. The NPS float number is in italics to the right of the mean depth, and the number of daily pressure values used to determine the statistics is below the variance bar. The depth for NPS14 was estimated from the temperature record. The depth variability is placed at the launch date for each float.



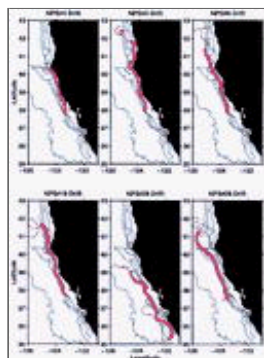
[Click on thumbnail for full-sized image.](#)

Fig. 5. Ensemble spaghetti diagram showing the smoothed subsurface trajectories of all the NPS RAFOS floats. The launch sites are indicated by circles, and the location where each float surfaced is indicated with an “x.” The float number is placed at the surfacing location. Depth shading is keyed to isobaths at 200, 1000, 2000, and 4000 m.



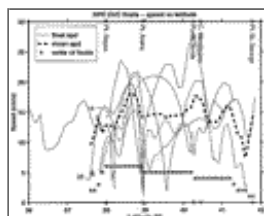
[Click on thumbnail for full-sized image.](#)

Fig. 6. Ensemble and individual spaghetti plots for the California Undercurrent flow regime. The undercurrent segment is drawn as a heavy line in the ensemble panel. In the individual



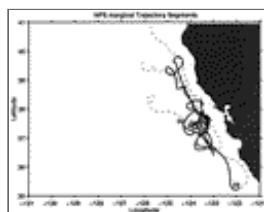
[Click on thumbnail for full-sized image.](#)

Fig. 6. (*Continued*) panels the daily positions are indicated by the red symbols. Isobaths for 200, 1000, 2000, and 4000 m are drawn in blue in the individual panels.



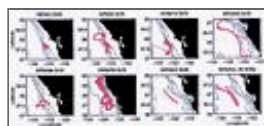
[Click on thumbnail for full-sized image.](#)

Fig. 7. Plot of float speed ( $\text{cm s}^{-1}$ ) vs latitude for the NPS RAFOS floats caught in the undercurrent. The thin solid lines show individual float daily speeds with float number is given at the start latitude. The thick dashed line is the mean speed. The asterisks give the number of floats used to determine each mean. The major coastal promontories are labeled at the top of the figure and indicated by open circles at the top and bottom of the figure.



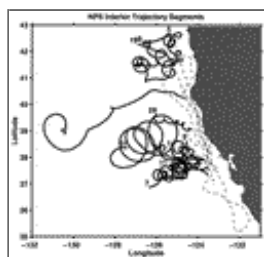
[Click on thumbnail for full-sized image.](#)

Fig. 8. As in [Fig. 6](#) but for the continental margin flow segment.



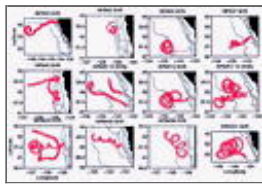
[Click on thumbnail for full-sized image.](#)

Fig. 8. (*Continued*)



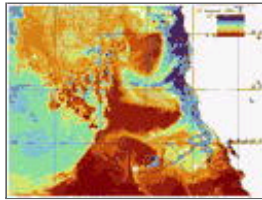
[Click on thumbnail for full-sized image.](#)

Fig. 9. As in [Fig. 6](#) but for the interior Pacific flow segment.



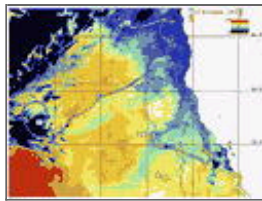
Click on thumbnail for full-sized image.

Fig. 9. (Continued)



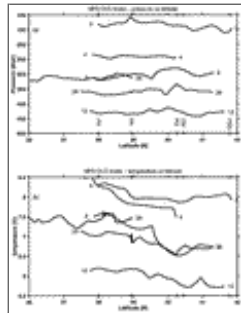
Click on thumbnail for full-sized image.

Fig. 10. Satellite imagery for 27 August 1993, with float trajectories for NPS 3, 5, and 7 superimposed. The dots are the daily interpolated float positions. The float position on the day of the satellite overpass is marked by a large black dot.



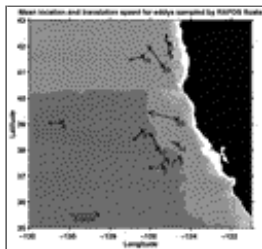
Click on thumbnail for full-sized image.

Fig. 11. Satellite imagery for 15 November 1993, with float trajectories for NPS 4, 8, and 10 superimposed. The dots are the daily interpolated float positions. The float position on the day of the satellite overpass is marked by a large black dot.



Click on thumbnail for full-sized image.

Fig. 12. Pressure (a) and temperature (b) plotted against latitude for the six float segments in the California Undercurrent. Float identification numbers are printed at the beginning and end of each segment. The major coastal promontories indicated in [Fig. 7](#) are again identified by open circles on the latitude axes and labeled with initials.



Click on thumbnail for full-sized image.

Fig. 13. The mean trajectory of each eddy sampled by the NPS RAFOS floats. The number at the base of each vector is the first float to encounter the eddy as listed in [Table 3](#). The origin of each vector is the location where the eddy was first encountered.

\* Current affiliation: Taygeta Scientific, Monterey, California.

*Corresponding author address:* Dr. Newell Garfield, Department of Geosciences, San Francisco State University, 1600 Holloway Ave., San Francisco, CA 94132.

E-mail: [garfield@sfsu.edu](mailto:garfield@sfsu.edu)

top ▲



© 2008 American Meteorological Society [Privacy Policy and Disclaimer](#)  
Headquarters: 45 Beacon Street Boston, MA 02108-3693  
DC Office: 1120 G Street, NW, Suite 800 Washington DC, 20005-3826  
[amsinfo@ametsoc.org](mailto:amsinfo@ametsoc.org) Phone: 617-227-2425 Fax: 617-742-8718  
[Allen Press, Inc.](#) assists in the online publication of AMS journals.